ELSEVIER

Thin Solid Films 342 (1999) 167–173

thin solid films

Free-carrier plasma resonance effects and electron transport in reactively sputtered degenerate ZnO:Al films

S. Brehme[a], F. Fenske[a], W. Fuhs[a], E. Nebauer[b], M. Poschenrieder[a], B. Selle[a,*], I. Sieber[a]

[a]*Hahn-Meitner-Institut Berlin (Abt. Photovoltaik), Germany*
[b]*Ferdinand-Braun-Institut für Höchstfrequenztechnik, Rudower Chaussee 5, D-12489 Berlin, Germany*

Received 17 June 1998; accepted 10 October 1998

Abstract

The electrical and infrared optical properties of reactively d.c. sputtered polycrystalline ZnO:Al films grown at varying oxygen flow rates were studied on samples prepared in the same deposition run. The carrier concentrations determined by Hall measurements were in the degeneration range. Relating them with the optical free-carrier resonance frequencies the effective electron mass was higher than in non-degenerate ZnO. The values of the optical mobility, calculated from the Drude damping factor, and of the Hall mobility were in the same order of magnitude. This suggests that the low carrier mobility in these films is mainly caused by scattering processes taking place within the film grains and that grain boundary scattering plays a minor role.

Keywords: Electrical properties and measurements; Infrared spectroscopy; Structural properties; Zinc oxide

1. Introduction

Thin films of highly conducting ZnO:Al are of current technological interest, e.g. for use as transparent contacts (TCO) in photovoltaic solar cells [1,2]. Reactive d.c. magnetron sputtering in an Ar/O_2 atmosphere providing reasonably high growth rates has emerged as a standard deposition method. For this technique, the dependence of the structural, electrical and optical properties on the deposition parameters has been comprehensively studied [2–6]. It is well known that the oxygen partial pressure during deposition is one of the most critical parameters in determining the resistivity and the optical transmission of the ZnO:Al films. The carrier concentration decreases with increasing oxygen flow rate $f(O_2)$ whereas the mobility goes through a maximum. The film resistivity can be minimized at comparatively low values of $f(O_2)$. This results, however, in a significant loss of optical transmission due to free-carrier absorption. For the application as TCO, there exists an optimum range of $f(O_2)$ where the most favourable balance between the divergent requirements of low film resistivity and high optical transmission can be achieved.

The structure of such films is rather complex. In general, columnar growth is observed with typical column diameters of 10 to 30 nm. It has been shown that these columns, which extend over the entire film thickness, consist of crystallites with significantly smaller size [7]. In such a heterogeneous system the comparison of electrical and infrared optical measurements can help to give useful insight into the transport limiting processes. In contrast to standard d.c. methods, the measurement at optical frequencies presents an alternative access to the study of carrier scattering processes by monitoring the electronic transport at a.c. conditions during very short periods of the carrier drift motion [8]. Thus, the electronic transport might be probed within dimensions which are smaller than the grain sizes.

The present paper, therefore, aims at a detailed study of the d.c. transport and of the free-carrier absorption in the infrared (IR). We will show that also in magnetron sputtered ZnO:Al films the square-root dependence of the plasma frequency on the carrier concentration, as predicted by the Drude theory, is valid. It is attempted to relate the experimental results with the structure of the films by comparing optical mobilities and Hall mobilities. It will be shown that in-grain scattering processes dominate the carrier transport in these films whereas the scattering effect of grain boundaries is less important.

2. Experimental procedure

The ZnO:Al films were produced by reactive d.c. magne-

* Corresponding author. Tel.: +49-30-67053-313; fax: +49-30-67053-333.
E-mail address: selle@hmi.de (B. Selle)

0040-6090/99/$ - see front matter
PII: S0040-6090(98)01490-4

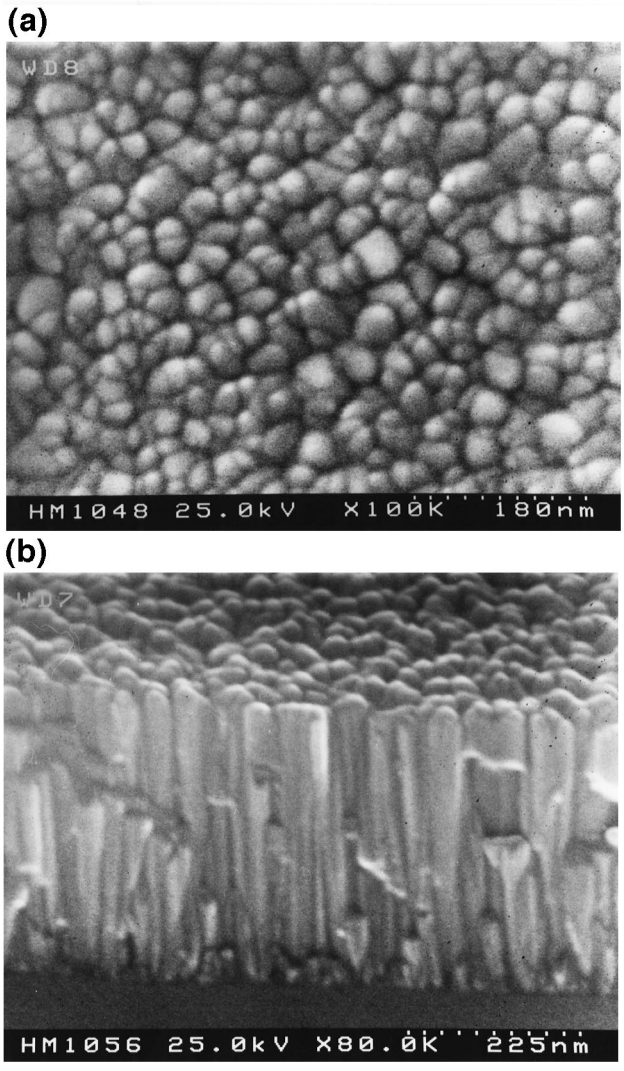

Fig. 1. SEM surface (a) and cross-section (b) micrographs of a ZnO:Al film on SiO_2/Si grown at $f(O_2) = 16$ sccm.

tron sputtering from a circular metallic compound Zn:Al(2 wt.%) target, 90 mm in diameter, in a sputtering-up configuration (55 mm distance from the substrate). The composition of the sputtering atmosphere, consisting of 6N purity Ar and O_2, was regulated by mass flow controllers. A high pumping rate was applied to prevent instabilities of the plasma discharge. For the experiments described below a special series of samples was prepared by varying the oxygen flow rate $f(O_2)$ between 0 and 32 sccm (standard cubic centimeter per minute). The discharge power and the total pressure were kept constant at near-optimum conditions established for our sputtering system (100 W and 6×10^{-3} mbar) [9]. During the deposition process, the substrates were not heated, and no additional bias was applied. The variation of $f(O_2)$ resulted in films of different carrier concentration, resistivity, and optical transmittance offering an adequate range of these properties for a comparative study. In accordance with the results reported in [4] the deposition rate decreased from 2 to 0.85 nm/s with increasing $f(O_2)$. With a deposition time of 200 s, the thicknesses of our films ranged between 170 and 400 nm. For a consistent comparison of the various film properties it was crucial to measure all relevant data on films grown in the same deposition run on the same substrate. We used Si wafers coated with about 400 nm standard thermal SiO_2 as a substrate in order to meet the requirements for the electrical, optical and structural measuring methods. Rutherford Backscattering Spectrometry (RBS) and optical measurements, which did not need contacts, were performed on identical sample pieces. All measurements were carried out on samples in their as-grown state, i.e. the films were not annealed after deposition.

Structural properties of the films were studied by 3° glancing incidence X-ray diffraction (XRD) and by scanning electron microscopy (SEM). The electron microscope was equipped with a field emission cathode and provided a resolution of at least 2 nm. The film composition, i.e. the atomic concentrations of Zn, O and Al, respectively, was analyzed by RBS with 1.4 MeV $^4He^+$ ions. For the determination of the concentrations the RBS spectra were fitted by an iterative computer simulation program based on the formalism given in [10]. Depth profiles of the film components were recorded by Secondary Ion Mass Spectrometry (SIMS) in a Cameca IMS4F system using 10 keV Cs^+ primary ions. The film thicknesses were derived from SEM cross-sectional views and from the RBS analysis. The infrared optical properties were studied by recording the reflectivity at 10° beam incidence with a Fourier-Transform Infrared (FTIR) spectrometer in the range between 400 and 15600 cm^{-1} (resolution < 2 cm^{-1}) and using Au and Al mirrors as a reference. All these studies were performed at room temperature. Resistivity, carrier concentration and mobility were determined by van der Pauw and Hall measurements in the temperature range 12–300 K.

3. Results

3.1. Structural properties and composition

XRD spectra and SEM micrographs indicate that for $f(O_2) \geq 12$ sccm the films grow strongly textured in a columnar structure with the hexagonal c-axis perpendicular to the substrate surface. Typical SEM images are shown in Fig. 1. When the columnar structure appeared, the dominant XRD peak was the (002) reflex at 34.4°. The (002) peak width was evaluated by the Scherrer formula following the usual approach as exemplified e.g. in [11]. Ignoring any effect of microstrains a nearly constant crystallite size of at least 85 ± 10 nm was obtained for all $f(O_2) > 14$ sccm. This value, which should indicate the mean grain dimension along the axial direction of the columns, was in some contrast to the column heights which, by the inspection of the cross-sectional SEM views (see Fig. 1b), appeared not much smaller than the film thickness. However, a detailed

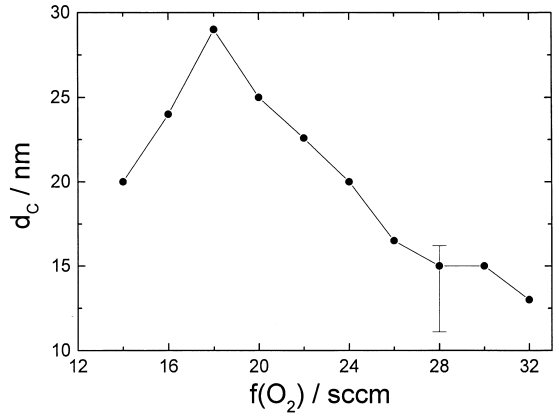

Fig. 2. Average column diameter d_c as a function of the oxygen flow rate $f(O_2)$. The error bar is representative for all data points.

TEM investigation of individual columnar grains has shown that, in fact, these are composed of slightly tilted crystallites having axial dimensions well below the visible column height [7]. The average value of the column diameters, which was determined by a statistical analysis of the SEM micrographs, depends on $f(O_2)$ attaining a maximum of 30 nm at 18 sccm and decreasing to the 15 nm level for higher oxygen flows (Fig. 2).

In Fig. 3 a representative RBS spectrum of a ZnO:Al film is plotted in a logarithmic scale in order to show the signal contribution of the Al dopant (channels 100 to 130). The total amount [Al] of the incorporated Al atoms, calculated from the Al signal height, was approximately within the same range between 1.2 and 1.5×10^{21} cm^{-3} for all films. The oxygen content approached a constant level slightly above 50 at.% for $f(O_2) \geq 14$ sccm. For low $f(O_2)$, a strong Zn excess was found, in accordance with the XRD patterns which indicated contributions of metallic Zn for these films. In the following, we will focus on the samples prepared with $f(O_2) \geq 14$ sccm. Cross-checks made by SIMS established the homogeneous depth distribution of Al, Zn and O. Weak signals of Ca^{40} and Ca^{44} in their correct isotopic ratio made

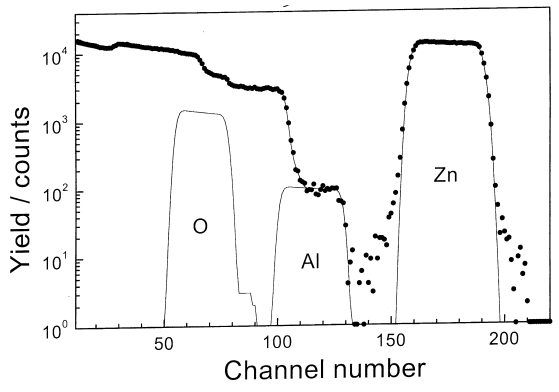

Fig. 3. RBS spectrum of a ZnO:Al film (thickness: 200 nm) on SiO_2(400 nm)/Si measured with 10 μC $^4He^+$ ions at 1.4 MeV and 5° beam incidence. Solid lines represent simulation fits for the complete structure and separately for the ZnO:Al film.

the SIMS analysis of Ar difficult. A detectable excess in the intensity of mass 40, which would indicate an Ar contamination above $\approx$ 0.2 at.%, was not observed. From the RBS spectra the thicknesses of the ZnO:Al films were determined by evaluating the width of the Zn signal peak and the position of the shifted Si edge (in the example of Fig. 3 at channel 100). The nearly perfect fit of the low-energy Zn peak edge suggests that the ZnO:Al films are fairly smooth (surface roughness $<$ 10 nm).

3.2. Electrical properties

Room temperature four-point probe and van der Pauw measurements revealed a resistivity minimum of about 6×10^{-4} Ω cm at $f(O_2) = 16$ sccm which was similar to the behaviour reported by others [3,4]. This minimum is accomplished by a strong decrease of the electron concentration, n, with increasing $f(O_2)$ and by the mobility maximum at about 18 sccm (Fig. 4). Since we have found by RBS that the total amount [Al] of the incorporated Al atoms is nearly constant for all films the decrease of the carrier concentration indicates a dramatic reduction of the Al doping efficiency n/[Al] from 0.85 at $f(O_2) = 12$ sccm down to about 10^{-3} at $f(O_2) = 32$ sccm.

Fig. 5 presents the temperature dependence of the electrical data. For all films the electron concentration was independent of temperature (Fig. 5b) which is characteristic for degenerate semiconductors. No freeze-out effect could be observed down to 12 K, and in almost all of the samples the Hall mobilities were also independent of temperature. Only the films with the lowest electron concentrations, which were grown at the highest oxygen flow rates ($f(O_2) = 30$ and 32 sccm, respectively), showed a weak dependence of the mobility on the temperature. For these films, the increase of the resistivity at lower temperatures was essentially due to the slight decrease of the mobility (compare Fig. 5a,c).

3.3. IR reflectance and Drude parameters

The optical reflectivity in the infrared was measured in order to determine the Drude parameters of the ZnO:Al films. These are involved in the classical oscillator model for free carriers where the real part ϵ_1 of the dielectric function can be written as

$$\varepsilon_1(\omega) = \varepsilon_\infty - \frac{\omega_p^2}{\omega^2 + \gamma^2} \quad (1)$$

Here, $\epsilon\infty$ is the high-frequency dielectric constant including the interband contribution, γ the damping constant and ω_p the plasma frequency which is related to the electron concentration n by

$$\omega_p = 2\pi c \nu_p = \left(\frac{ne^2}{\varepsilon_0 \varepsilon_\infty m^*} \right)^{1/2} \quad (2)$$

where ν_p is the plasma wavenumber, c is the light velocity, e

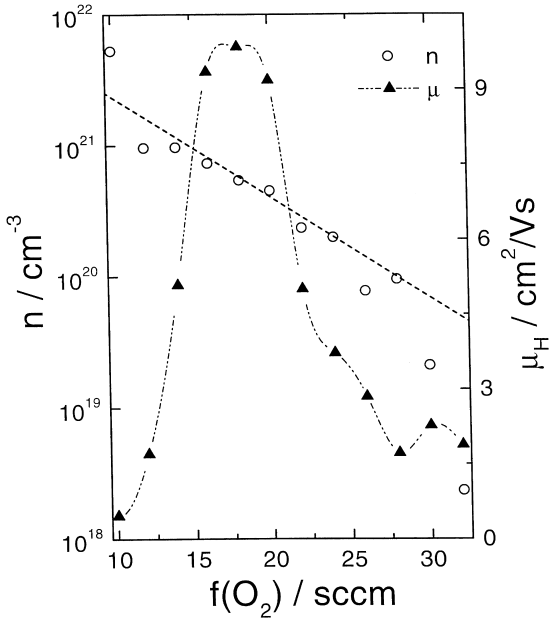

Fig. 4. Room-temperature electron concentration n and Hall mobility μ_H as a function of the oxygen flow rate f(O_2).

is the electron charge, ϵ_0 is the vacuum permittivity, m^* is the effective electron mass.

The reflectivity spectra of three samples prepared at low,

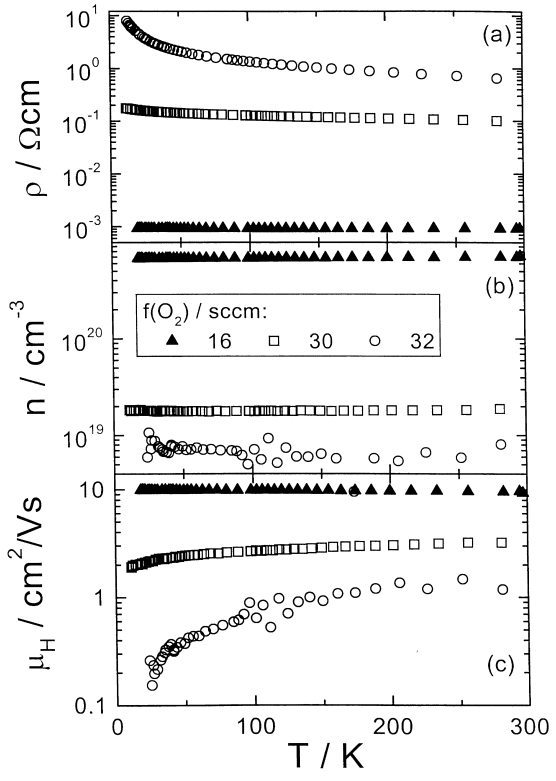

Fig. 5. Temperature dependence of the resistivity ρ (a), the electron concentration n (b) and the Hall mobility μ_H (c) for ZnO:Al films grown at a lower (16 sccm) and at the two highest (30 and 32 sccm) oxygen flow rates f(O_2).

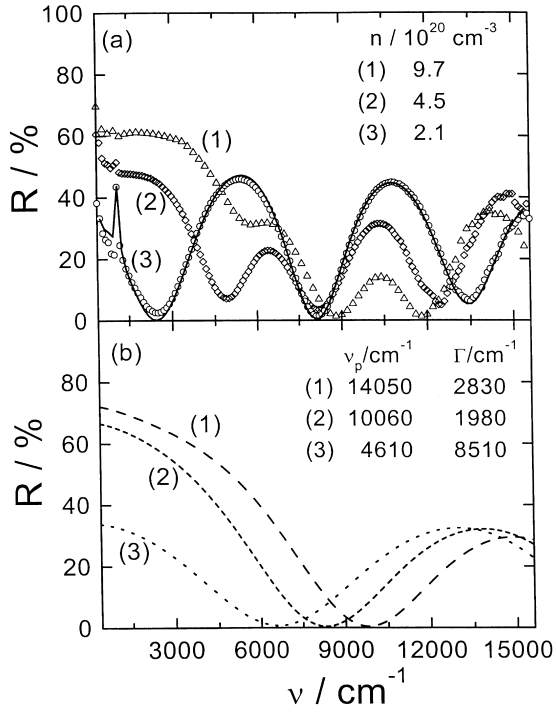

Fig. 6. (a) Optical reflectivity of three ZnO:Al/SiO_2/Si structures; $f(O_2)$ = 14 sccm (1), 20 sccm (2), 30 sccm (3). The solid line is an example of a simulation fit curve to (3). (b) Reflectivity curves for the same ZnO:Al films as shown in (a) but without the intermediate SiO_2 film. The curves were recalculated by using the indicated fit parameters for (1), (2) and (3), respectively ($\Gamma = \gamma/2\pi c$).

medium, and high $f(O_2)$ are shown in Fig. 6a. Although in these spectra the underlying SiO_2 film produces characteristic interference oscillations the free-carrier effects originating from the ZnO:Al film are clearly seen. The narrow spike at 1080 cm^{-1} is due to the Si–O–Si asymmetric-bond-stretching mode in the SiO_2 film. This structure becomes less pronounced with increasing carrier concentration in the ZnO:Al film because of the stronger attenuation by the free-carrier absorption in the upper ZnO:Al layer. The same effect also results in a decrease of the amplitude of the interference fringes arising from the underlying SiO_2.

For the calculation of the Drude parameters, the experimental spectra were fitted by an iterative simulation using the program ''SCOUTFIT'' [12,13]. A representative simulation, which proves the excellent fit to the data points, is shown in Fig. 6a by the full line. The samples were treated as a two-layer stack of SiO_2 and ZnO on a semi-infinite crystalline Si substrate in air. The stack boundaries were assumed as ideally flat which is justified by the RBS measurements (see Section 3.1). The presence of any voids or additional phases, formed e.g. by the adding of the Al dopant to ZnO, was neglected, and the optical properties of the films were considered to be homogeneous in depth. The simulation needs optical data of the crystalline Si and of the SiO_2 film as an input which were taken from standard tables [14]. For ZnO the dielectric background (i.e. the low-carrier-density limit) was kept constant at $k = 0$ and

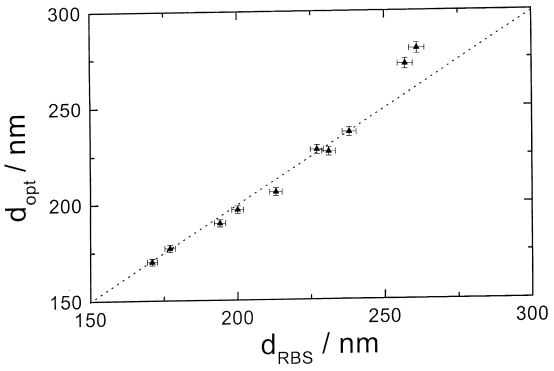

Fig. 7. Comparison of the ZnO:Al film thickness d_{RBS} determined by RBS with d_{opt} obtained by the simulation fit of the optical reflectivity spectra.

$\epsilon\infty = 4$ [15]. For the SiO_2 thickness a reference value, obtained by ellipsometry of the SiO_2/Si substrate prior to deposition, was inserted. Thus, the simulation of the spectra involved only three fit parameters: the Drude quantities ν_p and Γ and the thickness d_{opt} of the ZnO:Al film. Since the ZnO:Al film thicknesses were already known from the RBS analysis (see Section 3.1) this third fit parameter was used for a quality proof of the simulation. Taking advantage of the fact that optical and RBS techniques are based on quite different physical principles a comparison of the optical and RBS thicknesses is an appropriate check for the consistency of the IR spectrum simulation. In Fig. 7 the optical thicknesses of the ZnO:Al films derived from the fit procedure are plotted against the RBS thicknesses. With the exception of two samples all the thickness values agreed within a standard deviation of $\pm$ 2.3% thus indicating an acceptable accuracy of the fit results.

The best-fit values of the Drude parameters ω_p and γ (in Fig. 6 expressed by their wavenumber equivalents ν_p and Γ, respectively) were used to recalculate theoretical reflection spectra of the corresponding ZnO:Al single layers on Si, i.e. of hypothetical samples without the intermediate SiO_2 film. Three examples of such spectra, which more clearly show the shift of the plasma edge and the reflectivity minimum as a function of the carrier concentration, are plotted in Fig. 6b.

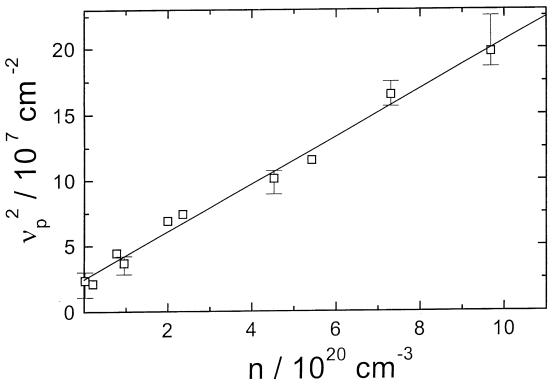

Fig. 8. Square of the plasma resonance wave number ν_p as a function of the electron concentration n.

Next, we relate the electrical and the IR optical properties. Fig. 8 presents the linear relationship of ν_p^2 and the carrier concentration n as predicted by Eq. (2). The offset of the line indicates a systematic deviation which most probably is caused by neglecting the influence of the optical phonon modes of ZnO [15,16] in Eq. (1). The slope of the line amounts to 1.8×10^{-13} cm. This is significantly lower than the value of 3.2×10^{-13} cm which would result from Eq. (2) with the effective electron mass $m^* = 0.28m_0$ of non-degenerate bulk ZnO [15]. The slope of the line in Fig. 8 yields a higher effective electron mass of $m^* = 0.50 \pm 0.05m_0$ for our films which may be understood on the background of the degeneracy and a possible non-parabolicity of the ZnO conduction band. Investigating the shift of the optical band gap Sernelius et al. [17] have shown that in highly doped ZnO:Al films the conduction band will be filled up at electron concentrations above 10^{20} cm^{-3}. If the band is non-parabolic then the value of m^* may increase with n. In fact, Minami et al. [18] arrived at a best quantitative fit of their experimental mobility data on ZnO:Al films when both the effects of the degeneracy and the non-parabolicity of the conduction band were taken into account. In addition, there could be influence of disorder at high carrier concentrations such as tail state formation.

The Drude damping factor γ can directly be related to the scattering mechanism of the carriers. Interpreting the reciprocal value $1/\gamma$ straight forwardly as an average collision time $\langle\tau\rangle$ of the electrons [8] an ''optical'' mobility μ_{opt} can be defined by

$$\mu_{opt} = e\langle\tau\rangle/m^* = e/m^*\gamma \quad (3)$$

This optical mobility μ_{opt} was calculated from the experimental values of the damping constant with $m^* = 0.50m_0$ resulting from Fig. 8. The Hall mobility μ_H and the optical mobility μ_{opt} are compared in Fig. 9. The most intriguing fact is that for all films μ_H and μ_{opt} are of the same order of magnitude. The measured values are rather low and in accordance with the data published in [6,18,19] for highly Al doped ZnO films. They are much smaller than the mobilities reported for non-degenerate bulk ZnO [20,21]. Comparing the shape of the curves with Fig. 2, a parallel dependence of the mobilities and the column diameter d_c on $f(O_2)$ can be stated. In particular, all these quantities have their maximum values at $f(O_2) = 18$ sccm. This suggests some common correlation of the columnar structure and the carrier mobility on the oxygen partial pressure during the film growth.

4. Discussion

In Al doped ZnO films the high carrier concentrations are mainly attributed to the contribution of shallow donors which are formed by substitutional incorporation of Al on a regular Zn lattice site [19]. In addition, conduction electrons can be supplied by intrinsic native defects (oxygen

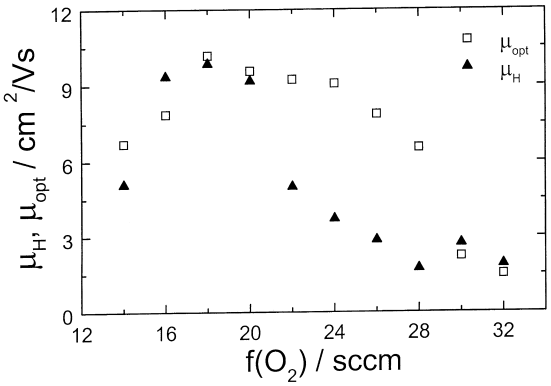

Fig. 9. Hall mobility μ_H and optical mobility μ_{opt} as a function of the oxygen flow rate $f(O_2)$.

vacancies V_O or interstitial zinc Zn_i) [22,23]. Our experimental results and those of others [3–6] show that the adequate incorporation of the Al atoms in a substitutional configuration depends crucially on the oxygen partial pressure, probably due to the influence of the oxygen on the impact and reaction kinetics in the sputtering process. Whereas the total amount of Al determined by RBS was always constant in our films the carrier concentration varied strongly with the oxygen flow and indicated a dramatic lowering of the Al donor activation efficiency with higher oxygen flow. This is quite in contrast to the expectations of the equilibrium defect chemistry of ZnO where a shift to oxygen-rich conditions should increase the number of Zn vacancies, enhance the site offer for the Al donors and, thus, raise the doping efficiency [22]. The observed trend in our films would only agree with equilibrium models if the role of the Al atoms as a dopant is assumed to be negligible. In this case, the electron concentration would be expected to decrease at oxygen-rich growth conditions where the formation of V_O or Zn_i will be much less probable.

In any of these options one is faced to the fact that increasingly high concentrations of ''neutralized'' Al atoms, which are not adequately incorporated to be donor active, are present in the ZnO:Al films sputtered under oxygen-rich conditions. By means of a principal component analysis of the Auger spectra we have found recently that a considerable amount of the Al in our films prepared at high $f(O_2)$ is bonded to oxygen in an Al_2O_3 configuration [24]. Therefore, we believe that the oxidation of Al, as it was suspected previously in [4], is the main competing process for the formation of a substitutional Al donor. The resulting Al oxide complexes, although not contributing to the carrier concentration, cannot be excluded to influence the carrier scattering and to be a possible reason for the low carrier mobilities in films sputtered at higher oxygen partial pressure.

An important conclusion on the electronic scattering may be drawn from the comparison of the optical and the Hall mobilities. The Hall mobility μ_H is measured under d.c. conditions and should involve all scattering processes which control the lateral electron transport in the film including especially the scattering at the grain boundaries. The optical mobility μ_{opt}, on the other hand, is obtained by sampling the carrier motion at optical frequencies where the monitored transport paths are smaller than the grain size and, thus, the probability of crossing a grain boundary is low. One therefore expects that μ_{opt} is significantly larger than μ_H. This, however, was not found in the experiment. The coincidence of the Hall mobility and the optical mobility (see Fig. 9) indicates that both quantities are limited by the same scattering process taking place within the volume of the grains. The mean free path length of the electrons $l = v_{el} \times \langle \tau \rangle$ (v_{el} is the electron velocity) can be estimated by Eq. (3). Inserting $\mu = 10$ cm^2/Vs, $m^* = 0.5m_0$ and an electron velocity of the order 10^7 cm/s the electron mean free path is close to 1 nm and, in fact, well below the grain dimensions. Since the dominant scattering process being responsible for the low overall mobilities in our films occurs in the bulk of the film grains the grain boundary scattering turns out to play a minor role only.

The comparatively small influence of the grain boundary scattering is also concluded from the temperature dependence of μ_H shown in Fig. 5c. The absence of a thermal activation is a typical feature of the electronic transport in degenerate polycrystalline TCO films. This is because the carrier densities are in excess of 10^{20} cm^{-3} where the barrier thicknesses at the grain boundaries become as low that they can be penetrated by tunneling currents which do not depend on temperature [25]. Therefore, thermionic emission of the carriers across the grain boundaries has been shown to control the Hall mobility only in non-degenerate polycrystalline ZnO films where for electron densities $< 10^{18}$ cm^{-3} tunneling transitions are much less probable [23]. Applying the formalism of the thermionic emission theory [26,27] we evaluated the data from the sample grown at $f(O_2) = 32$ sccm, i.e. the sample with the lowest electron concentration, by a plot of $\ln(\mu_H/T^{1/2})$ over $1/T$. An effective barrier height of $E_{b,eff} = 15$ meV was obtained for the temperature range from 85 to 300 K. Although this value of $E_{b,eff}$ is lower than the thermal energy at room temperature the data points were well correlated. This suggests that the true barrier height is higher than the measured $E_{b,eff}$ and that this film represents a transitional case where the thermionic emission is partly replaced by tunneling processes. Thus, the total rate of electrons crossing the barrier is increased effectively and fakes a lower $E_{b,eff}$ if one neglects the tunneling contribution.

The low in-grain mobilities are in accordance with recent model considerations [18,25] which have shown that in degenerate TCO films the ionized-impurity scattering might be the dominant process reducing the electron mobility to a very low level with no significant temperature dependence. The dependence of μ on the carrier concentration n, in this case, should follow approximately a relationship of $\mu \propto n^{-2/3}$ [6,18,19] which was not observed in our films. The lowest mobilities were measured even in the films with the smallest carrier concentration. These were depos-

ited at high $f(O_2)$ and had the highest amount of inactive Al. Thus, it can be suspected that the in-grain mobility will be reduced additionally by the presence of the oxidized Al complexes which are likely to act as potential scattering centres. Mobilities below the $\mu \propto n^{-2/3}$ limit in the range of $n < 3 \times 10^{20}$ cm^{-3} were also reported in [6]. Assuming a neutral-defect scattering mechanism to be responsible for this effect a mobility smaller than 10 cm^2/Vs and a mean free path of a few nm only can be estimated for a defect density of about 10^{20} cm^{-3} [28]. This defect concentration is well in the range of the Al content in our ZnO:Al films that is not active as a donor.

5. Conclusions

This study has shown that the electrical and optical properties of highly doped ZnO:Al films, which are prepared by reactive d.c. sputtering, are dominated by electron concentrations in the degeneration range. The electron concentration depends dramatically on the oxygen flow rate during deposition. With increasing oxygen flows the donor efficiency of the incorporated Al atoms is diminished by a competing deactivation process, most probably Al oxidation. Comparing the electrical data with the optical plasma resonance parameters the predictions of the classical Drude model could be verified. A higher value of the effective electron mass with respect to the bulk effective mass reported in the literature has been found. It can be explained by the influence of the degeneracy and the non-parabolicity of the ZnO conduction band or by the high degree of structural disorder in the films. The optical a.c. mobility derived from the Drude damping factor agrees with the measured d.c. Hall mobilities. This result, together with the temperature dependence of the electrical data, leads to the conclusion that the mobility in our polycrystalline ZnO:Al films is limited mainly by in-grain scattering processes while grain boundary scattering is less effective due to electron penetration of the grain boundary barriers by tunneling transitions.

Acknowledgements

The authors are grateful to M. Trapp (RTG Mikroanalyse GmbH Berlin) for performing the SIMS analysis. This work was supported in part by the Bundesministerium für Bildung und Forschung (contract 0329773).

References

[1] W.H. Bloss, F. Pfisterer, M. Schubert, T. Walter, Prog. Photovolt.: Res. Appl. 3 (1995) 3.
[2] R. Schäffler, H.W. Schock, 23rd IEEE Photovolt, Specialists Conf., Louisville, , IEEE, Piscataway 1993 (1993) 1026.
[3] G.L. Harding, B. Window, E.C. Horrigan, Solar Energy Mater. 22 (1991) 69.
[4] K. Ellmer, F. Kudella, R. Mientus, R. Schieck, S. Fiechter, Thin Solid Films 247 (1994) 15.
[5] L.J. Meng, M.P. dos, S. antos, Thin Solid Films 250 (1994) 26.
[6] S. Zafar, C.S. Ferekides, D.L. Morel, J. Vac. Sci. Technol. A 13 (1995) 2177.
[7] I. Sieber, N. Wanderka, I. Urban, I. Dörfel, E. Schierhorn, F. Fenske, W. Fuhs, Thin Solid Films, (1997) to be published.
[8] J.F. Black, E. Lanning, S. Perkovitz, Infrared Phys. 10 (1970) 125.
[9] S. Brehme, L. Elstner, F. Fenske, et al., 13th Eur, Photovoltaic Solar Energy Conf., Nizza, , Stephens, Bedford 1995 (1995) 1746.
[10] W. -K, Chu, J.W. Mayer, M.-A. Nicolet, Backscattering Spectrometry, Academic Press, Boston, , p. (1978) 87.
[11] L.J. Meng, M.P. dos, S. antos, Thin Solid Films 226 (1993) 22.
[12] W. Theis, RWTH Aachen, 1995, private communication.
[13] P. Grosse, in: R. Helbig (Ed.), Festkörperprobleme, 31, Vieweg, Braunschweig, 1991, pp. 77.
[14] E.D. Palik (Ed.), Handbook of Optical Constants of Solids Academic Press, Orlando, 1985, pp. 547.
[15] H. Weiss, M. Schulz, O. Madelung (Eds.), Numerical Data and Functional Relationships in Science and Technology *Landoldt–Börnstein New Series*, 17b, Springer-Verlag, Berlin, 1982, pp. 35.
[16] M. Göppert, F. Gehbauer, M. Hetterich, J. Münzel, D. Queck, C. Klingshirn, J. Luminescence 72 (1997) 430.
[17] B.E. Sernelius, K. -F, Berggren, Z.-C. Jin, I. Hamberg, C.G. Granqvist, Phys. Rev. B 37 (1988) 10244.
[18] T. Minami, H. Sato, K. Ohashi, T. Tomofuji, S. Takata, J. Cryst. Growth 117 (1992) 370.
[19] T. Minami, H. Sato, H. Nanto, S. Takada, Jpn. J. Appl. Phys. 24 (1985) L781.
[20] P. Wagner, R. Helbig, J. Phys. Chem. Solids 35 (1974) 327.
[21] E. Ziegler, A. Heinrich, H. Oppermann, G. Stöver, Phys. Stat. Sol. A 66 (1981) 635.
[22] E. Kaldis, W. Hirschwald (Eds.), Current Topics in Materials Science, 7, North-Holland, Amsterdam, 1981, pp. 143.
[23] K. -S, Weiβenrieder, , J. Müller, Thin Solid Films 300 (1997) 30.
[24] A. Schöpke, F. Fenske, B. Selle, I. Sieber, Surf. Interf. Anal., 26 (1998) to be published.
[25] D.H. Zhang, H.L. Ma, Appl. Phys. A 62 (1996) 487.
[26] J.Y.W. Seto, J. Appl. Phys. 46 (1975) 5247.
[27] J.W. Orton, M.J. Powell, Rep. Prog. Phys. 43 (1980) 1263.
[28] T.C. McGill, R. Baron, Phys. Rev. B 11 (1975) 5208.